EVLA Memo #197
Techniques for Galactic Hɪ calibration from 21-SPONGE

Claire Murray (UW Madison), W. M. Goss (NRAO), Snežana Stanimirović (UW Madison)

July 1, 2016

Abstract

We report on the techniques and strategies developed for the VLA large project 21-SPONGE (21-cm SPectral Line Observations of Neutral Gas with the EVLA). These include instrument setup for calibration via frequency switching, filtering Hɪ emission by excluding short baselines and combining bandpass calibration observations in time. We display examples of the dynamic range in Hɪ absorption acheivable ($\sim 10^4$) thanks to these strategies and the upgraded WIDAR correlator.

1 Introduction

21-SPONGE (21-cm SPectral Line Observations of Neutral Gas with the EVLA) targeted bright ($S_{1.4\,\mathrm{GHz}} > 3\,\mathrm{Jy}$), compact radio continuum sources to measure absorption by intervening Hɪ in the local Galactic interstellar medium (ISM). Between 2011 and 2015, we accumulated over 500 hours of VLA time, mostly at C-priority with scheduling blocks (SBs) shorter than 1 hr. To detect signals from Hɪ at all densities and temperatures, we require extremely high sensitivity in Hɪ optical depth, reaching RMS noise levels of $\sigma_\tau \sim 5 \times 10^{-4}$ per $0.42\,\mathrm{km\,s^{-1}}$ channels, making 21-SPONGE the largest (55 sources) and most sensitive survey for Hɪ absorption to date.

2 Calibration Issues

Achieving such high sensitivity ($\sigma_\tau < 10^{-3}$ per channel) in Hɪ absorption requires careful attention to calibration. In this section, we describe several important calibration issues.

2.1 Contamination by HI at $v \sim 0\,\mathrm{km\,s^{-1}}$

In contrast to spectroscopy at most other radio wavelengths, it is difficult to calibrate observations at the Galactic Hɪ target frequency, namely, at LSR velocity $v_{\mathrm{LSR}} = 0\,\mathrm{km\,s^{-1}}$ (hereafter v). Absorption and emission by ambient Hɪ in the direction of any calibrator source will contaminate the calibration solutions because Galactic Hɪ is present at $v = 0\,\mathrm{km\,s^{-1}}$ nearly everywhere in the sky.

To resolve this issue, it is possible to calibrate at off-line frequencies. By observing bandpass calibrators at frequencies offset from $v = 0\,\mathrm{km\,s^{-1}}$, we can characterize the bandpass without incorporating the absorption or emission of Hɪ located in front of the calibrators into the solutions. We describe the instrument setup and calibration strategy below.
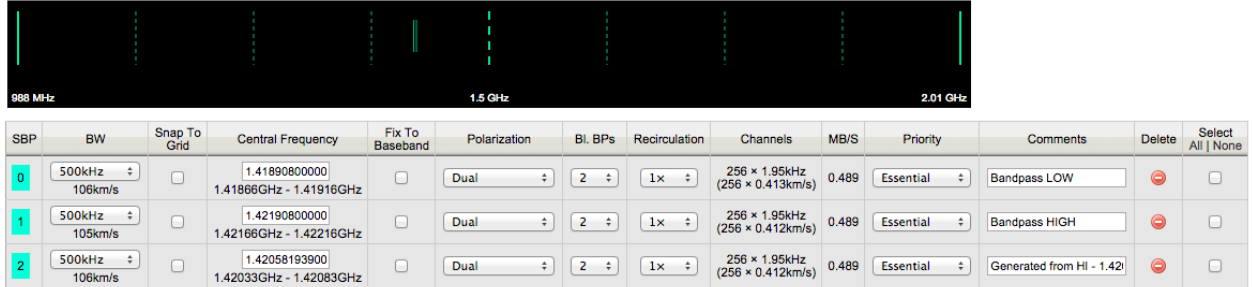
SBP	BW	Snap To Grid	Central Frequency	Fix To Baseband	Polarization	Bl. BPs	Recirculation	Channels	MB/S	Priority	Comments	Delete	Select All | None
0	500kHz 106km/s	☐	1.41890800000 1.41866GHz - 1.41916GHz	☐	Dual	2	1×	256 × 1.95kHz (256 × 0.413km/s)	0.489	Essential	Bandpass LOW	⊖	☐
1	500kHz 105km/s	☐	1.42190800000 1.42166GHz - 1.42216GHz	☐	Dual	2	1×	256 × 1.95kHz (256 × 0.412km/s)	0.489	Essential	Bandpass HIGH	⊖	☐
2	500kHz 106km/s	☐	1.42058193900 1.42033GHz - 1.42083GHz	☐	Dual	2	1×	256 × 1.95kHz (256 × 0.412km/s)	0.489	Essential	Generated from HI - 1.42(	⊖	☐

Figure 1: Instrument configuration display from the OPT. We perform bandpass calibration by frequency switching. The two 0.5 MHz bandpass calibration subbands, "high" and "low", are offset from the central HI observation subband by 1.5 MHz ($\sim 316\,\mathrm{km\,s^{-1}}$) in order to avoid HI absorption lines from the strong bandpass calibrators, resolved emission in the close array configurations, and increased system temperature noise from strong HI emission.

2.1.1 Frequency-Switched Calibration Setup

Our observations utilize three standard L-band configurations, each with one dual polarization IF of 0.5 MHz bandwidth with 256 channels (1.95 kHz channel spacing). We use two configurations, one centered at 1.421908 GHz (1.5 MHz, or about 316 km/s, higher than the HI rest frequency, called "high") and one at 1.418908 GHz (1.5 MHz lower, called "low") in order to perform bandpass calibration for HI line observations.

Following the recent upgrades to the WIDAR correlator, we were able to observe with all three instrument configurations (i.e. high, low and target HI line) simultaneously. Figure 1 displays the instrument configuration from the OPT.

For bandpass calibration, we favor the strong calibrators, 3C286 ($S_{1.4\,\mathrm{GHz}} = 15\,\mathrm{Jy}$), 3C147 ($S_{1.4\,\mathrm{GHz}} = 23\,\mathrm{Jy}$) and 3C48 ($S_{1.4\,\mathrm{GHz}} = 16.5\,\mathrm{Jy}$). As a C-priority project, we operate with short ($< 1\,\mathrm{hour}$) SBs, and therefore we must maximize efficiency (and minimize slew time). If a target is bright enough ($S_{1.4\,\mathrm{GHz}} \geq 6\,\mathrm{Jy}$), we use it as its own bandpass calibrator. This is possible given our small bandwidth (0.5 MHz). For a 6 Jy source, in order to reach rms noise levels of $\sim 5 \times 10^{-4}$, we need at least 3 hours of total integration time per bandpass calibrator.

2.2 Example: Observing Galactic Hi Absorption towards 4C12.50

As an example of how we perform bandpass calibration via frequency switching to avoid contamination by HI structure at $v = 0\,\mathrm{km\,s^{-1}}$, we consider an observation of the compact radio source 4C12.50 (RA=13:47:33, DEC=12:17:24; $S_{1.4\,\mathrm{GHz}} = 5.2\,\mathrm{Jy}$).

To measure HI absorption in the direction of 4C12.50 with an RMS noise in optical depth of $\sigma_\tau = 5 \times 10^{-4}$, we consult the exposure calculator to find that we need an on-source integration time of ~ 4.5 hours. Fortunately, 4C12.50 is a well-known calibrator source, and therefore can be used as its own complex gain calibrator throughout the observations. For bandpass calibration, we select the nearby well-known calibrator source 3C286 ($S_{1.4\,\mathrm{GHz}} = 15\,\mathrm{Jy}$). To achieve the required sensitivity, the exposure calculator indicates that we need at least 30 minutes of integration time on the bandpass calibrator.

With the ability to observe multiple subbands simultaneously, we observe all target and calibrator sources with the "high", "low" and target HI subbands simultaneously as described in
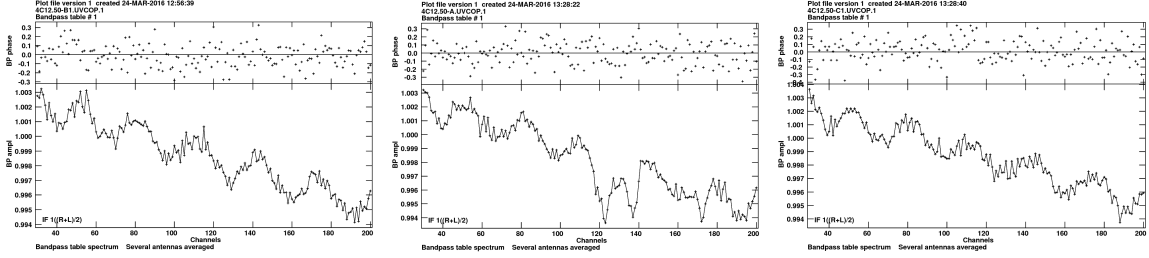
Figure 2: Left: BP solution constructed with observations of 3C286 in the "low" subband (see Figure 1 for the instrument setup); Center: BP solution constructed with observations of 3C286 at the target H I frequency; Right: BP solution constructed with observations of 3C286 in the "high" subband (see Figure 1 for the instrument setup). Extraneous bandpass structure at $v = 0\,\mathrm{km\,s}^{-1}$ from absorption by H I towards 3C286 is present at the H I frequency (central panel). The "ripple" present in all bandpass solutions is discussed in Section 4.

Section 2.1.1.

2.2.1 Bandpass Calibration of 3C286 via Frequency-Switching

Following observations and initial flagging, we calibrate the bandpass using the AIPS task BPASS with observations of 3C286. Given that our bandpass calibrator is a well-modeled source, we incorporate a model of the source during calibration. We compute the bandpass solution for the "low", target H I line, and "high" subbands and display the results in Figure 2. These plots were constructed using AIPS task POSSM with "APARM(8) 2" and are zoomed-in to the central channels (selected channesl 30 through 200 out of 256 total channels with "BCHAN 30; ECHAN 200") to display the amplitude structure of the bandpass in more detail. We note that there is a striking "ripple" structure with period $\sim 60\,\mathrm{kHz}$ period present in all bandpass solutions throughout this memo. We will address this structure and its cause in Section 4, and we previously discussed its properties in VLA Memo #171.

As shown in Figure 2, at the H I frequency (central panel), there is extraneous structure in the bandpass solution imposed by intervening H I absorption at $v = 0\,\mathrm{km\,s}^{-1}$ in comparison with the off-line frequencies (left and right panels). To avoid incorporating this structure into our target observation of source 4C12.50, we use the bandpass information from the "high" and "low" subbands (see Figure 1 for the instrument setups), rather than data from the target H I subband

After constructing BP solutions for the high and low subbands individually, we use the task BPLOT to examine the solution from each antenna separately and remove any noisy individual antennas. Finally, we combine the high and low subbands using the AIPS task DBCON and re-compute the BP solution with BPASS. This averaging process allows us to interpolate over the intervening target H I frequencies. The resulting BP solution, which contains accurate phase information for the target observation, is shown in Figure 3. This is the BP solution that we will apply to the target H I frequency observations of 4C12.50 later in the reduction process.

2.3 Spacing of Frequency-Switched Subbands

Given the WIDAR corrleator capability of including many subbands simultaneously, we experimented with different subband spacing above and below the H I rest frequency. Figure 4 displays a

screenshot of the OPT from an example test setup, including six subbands spaced by 1.5 MHz each above and below the target H I subband.

Using the same observation of 4C12.50 with calibrator 3C286 described in Section 2.2, we show example BP solutions constructed using various combinations of additional subbands spaced above and below the target H I line as shown in the setup from Figure 4.

Figure 5 shows the BP solutions from subbands spaced by 3 MHz (left) and 4.5 MHz (right) from the target H I line. By inspection, the solution does not change significantly with increased spacing from the target H I line.

Figure 6 shows BP solutions after combining two "low" and two "high" subbands (left; 4 total subbands combined) and after combining three "low" and three "high" subbands (right; 6 total subbands combined) on either side of the target H I line. By inspection the noise in the BP solution does not improve significantly between the two examples, and also does not improve significantly from the solution presented in Figure 3, which contains data from only two subbands.

Overall, increased subband spacing did not change the quality or stability of the calibration solutions. Furthermore, we found that combining data from multiple subbands does not significantly improve the noise in the bandpass solution.

2.4 Increased System Temperature

In addition to bandpass structure contamination at $v = 0\,\mathrm{km\,s^{-1}}$, strong emission by H I causes the system temperature (T_{sys}) to vary with frequency according to the strength of the emission. To display this effect, in the left panel of Figure 7 we show the scalar-averaged amplitude spectrum (with no calibration applied yet, generated with AIPS task POSSM) towards source J2136+0041 ($S_{1.4\,\mathrm{GHz}} = 3.3\,\mathrm{Jy}$). The structure reflects the variation of T_{sys} across the bandwidth, and ressembles the Galactic H I emission profile in this direction. For comparison, the brightness temperature spectrum in the direction of J2136+0041, from the Leiden-Argentine-Bonn (LAB) all-sky H I survey (angular resolution $\sim 36'$ [2]), is shown in the right panel of Figure 1.
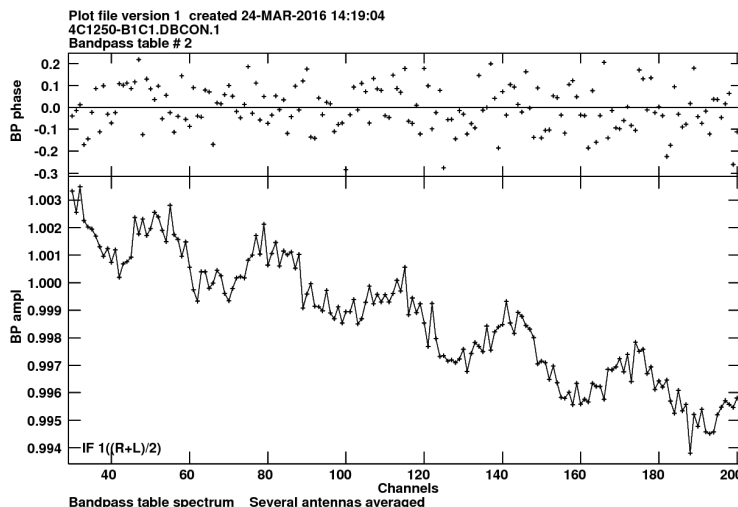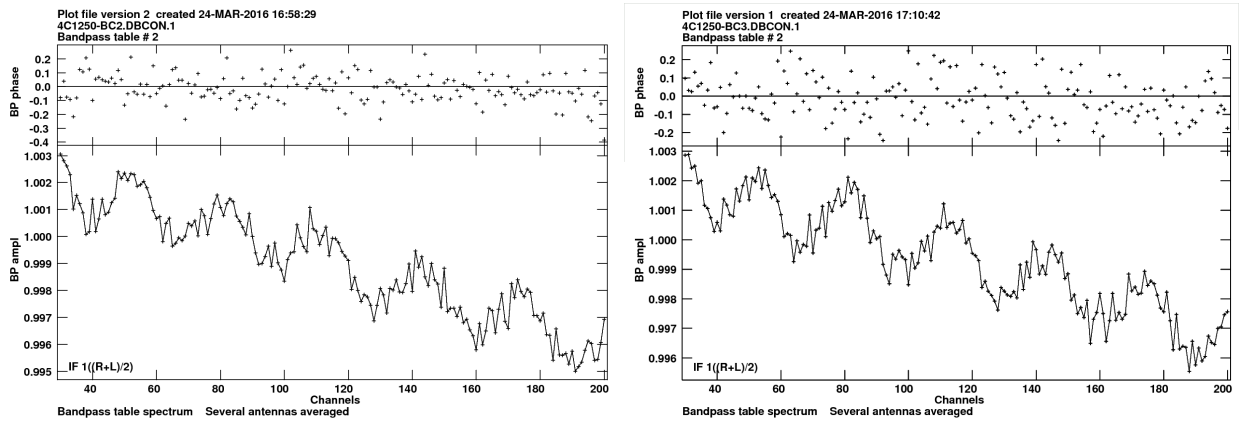

Figure 3: BP solution constructed with observations of 3C286 after combining data from the "low" and "high" subbands (see Figure 1 for the instrument setup).

Figure 4: Instrument configuration display from the OPT. Testing six 0.5 MHz subbands offset from the central H I observation subband by 1.5 MHz ($\sim 316\,\mathrm{km\,s^{-1}}$) each in order to avoid H I absorption lines from the strong bandpass calibrators, resolved emission in the close array configurations, and increased system temperature noise from strong H I emission.

2.5 Resolved HI Emission

In observations of radio continuum point sources designed to detect absorption by H I it is clear that the structure of H I emission along the line of sight is easily resolved on baselines of order ~ 100's of meters. At the H I frequency of 21 cm, this baseline length corresponds to $\sim 100\,\mathrm{m}/0.21\,\mathrm{m} = 0.5\,\mathrm{k\lambda}$, or kilo-wavelengths. We show an example of this effect in Figure 8. The left panel displays a vector-averaged spectrum towards the continuum source J2136+0041, observed during a hybrid array configuration between A and D arrays (and therefore includes several baselines $> 100\,\mathrm{m}$ in

Figure 5: Left: BP solution constructed with observations of 3C286 after combining data from subbands "low 2" and "high 2" (see Figure 4 for the instrument setup), spaced by 3 MHz from the target H I line; Right: BP solution constructed with observations of 3C286 after combining data subbands "low 3" and "high 3" (see Figure 4 for the instrument setup), spaced by 4.5 MHz from the target H I line. The "ripple" present in all bandpass solutions is discussed in Section 4.
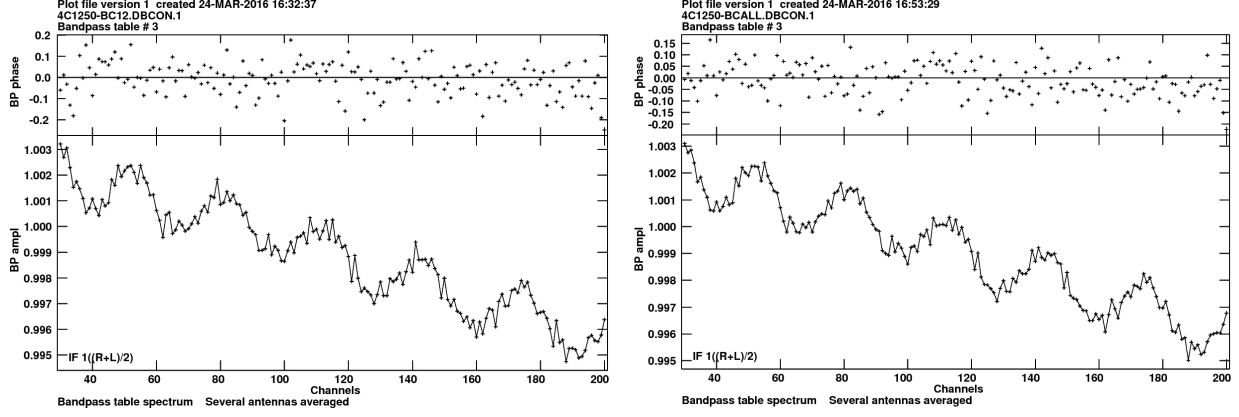
5

Figure 6: Left: BP solution constructed with observations of 3C286 after combining data from two "low" and two "high" subbands (see Figure 4 for the instrument setup); Right: BP solution constructed with observations of 3C286 after combining data from three "low" and three "high" subbands (see Figure 4 for the instrument setup). The "ripple" present in all bandpass solutions is discussed in Section 4.

length), with no calibration applied. The right panel displays the same plot with all baselines shorter than 300 m removed, which removes the resolved emission structure from the data.

After testing a range of minimum baselines, we have adopted 300 m as a baseline cutoff to ensure that most resolved emission structure is removed from the data without compromising sensitivity from the loss of too many baselines.

The effect of resolved emission on the fully-calibrated data is not as dramatic, but is still apparent. In Figure 9, we display two vector-averaged cross-power spectra of the same source, J2136+0041, following calibration with (left) and without (right) all baselines shorter than 300 m
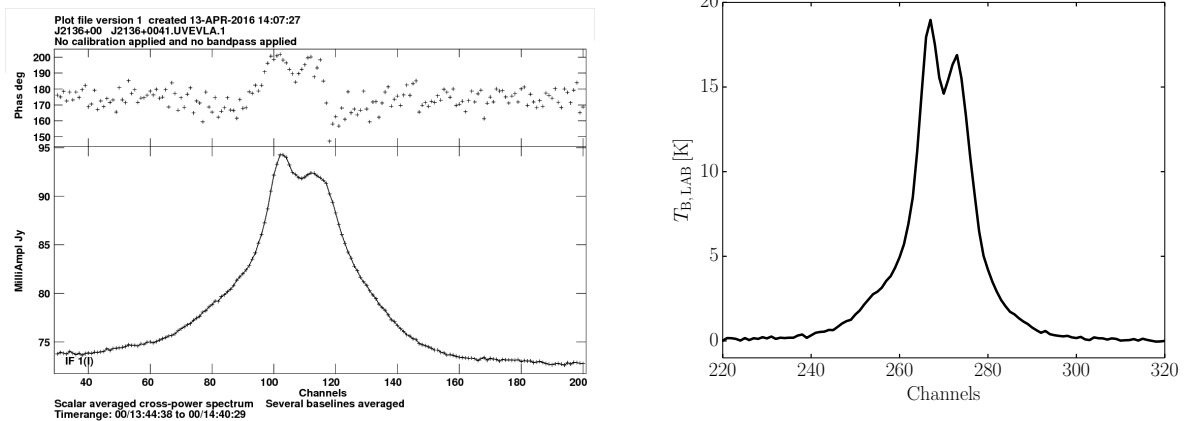

Figure 7: Left: Scalar averaged cross-power spectrum at the Hɪ frequency in the direction of source J2136+0041 with no calibration applied, constructed with the AIPS task POSSM and exported with LWPLA. Right: Brightness temperature spectrum towards source J2136+0041 from the LAB survey [2].
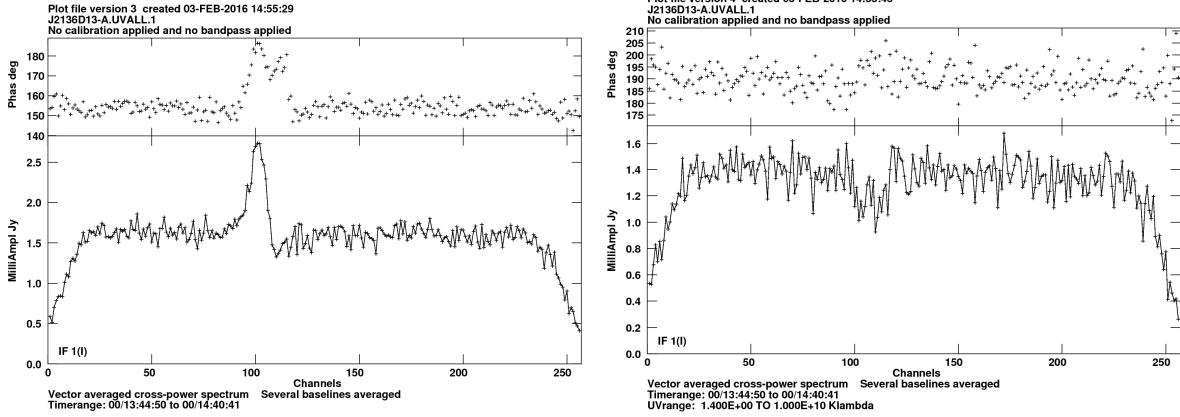
6

Figure 8: Left: Vector averaged cross-power spectrum at the H I frequency in the direction of source J2136+0041 ($S_{1.4\,\text{GHz}} = 3.3\,\text{Jy}$) with no calibration applied. Right: same as left, with baselines shorter than $300\,\text{m}$ (1.4 kilo-wavelengths) removed. Both plots constructed with the AIPS task POSSM and exported with LWPLA.

included. The depth of the absorption line at channel 100 in particular is significantly affected by resolved emission structure from the short baselines.

To remove data from baselines shorter than $300\,\text{m}$, we used the AIPS task UVCOP with setting "UVRAN 1.4 0" to select all baselines longer than $300\,\text{m} = 1.4\,\text{k}\lambda$.

3   Combining Calibration Observations in Time

To improve the noise level in the bandpass solutions further, we experimented with combining bandpass calibration observations spaced in time by intervals up to several days. We expect the
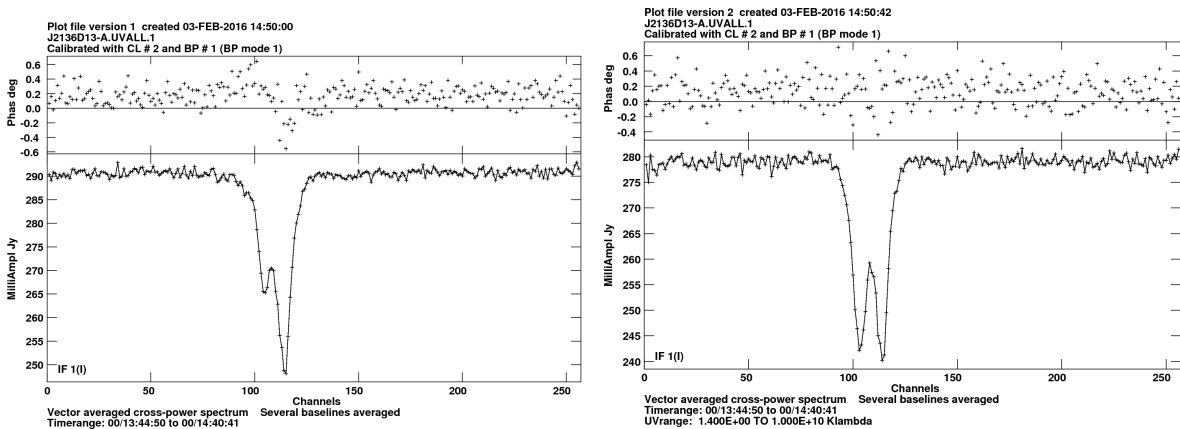

Figure 9: Left: Vector averaged cross-power spectrum at the H I frequency in the direction of source J2136+0041 ($S_{1.4\,\text{GHz}} = 3.3\,\text{Jy}$) with bandpass and gain calibration applied. Right: same as left, with baselines shorter than $300\,\text{m}$ (1.4 kilo-wavelengths) removed. Both constructed with the AIPS task POSSM and exported with LWPLA.
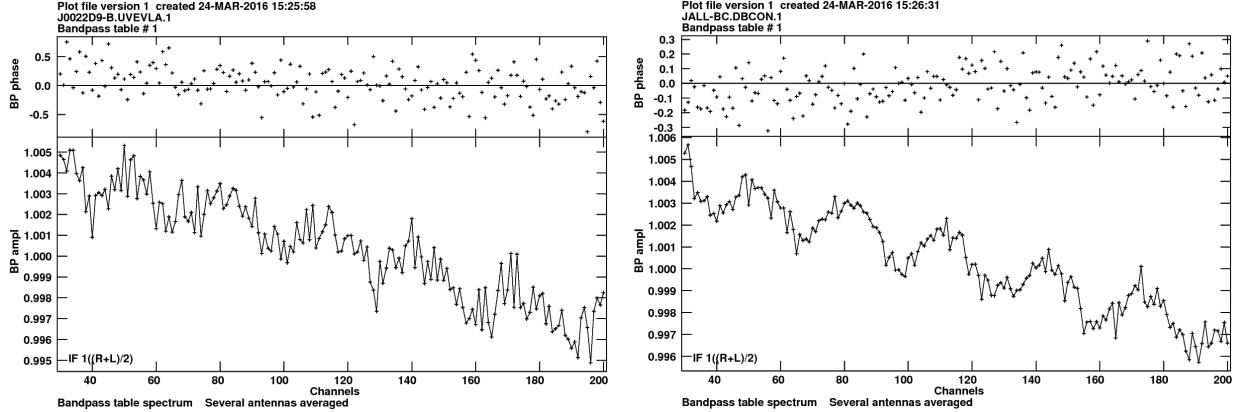
7

Figure 10: Left: BP solution constructed with observations of 3C48 in 10 minutes of integration time; Right: BP solution constructed by combining observations of 3C48 spaced in time by 4 months. The "ripple" present in all bandpass solutions is discussed in Section 4.

noise in the bandpass solution to decline according to the factor of increase in integration time (Δt) given by the ideal radiometer equation, or by $1/\sqrt{\Delta t}$. For example, we observed the source 3C147 ($S_{1.4\,\mathrm{GHz}} = 23\,\mathrm{Jy}$) twice on 2 consecutive days, with $33\,\mathrm{m}$ and $30\,\mathrm{min}$ of on-source integration time respectively. After combining the osebrvations, the increase in integration time relative to the first day is a factor of $\Delta t = 63/33 = 1.9$. Thereore, we expect the noise of the bandpass solution to improve by a factor of $1/\sqrt{\Delta t} = 1.38$. Following calibration, we found that the improvement in noise was $0.00073/0.00055 = 1.33$, which is nearly the theoretically expected amount.

In this process, we are able to combine observations of different sources. VLA Memo # 176 contains further details[4]. During our tests, we combined data from sources 3C410 ($S_{1.4\,\mathrm{GHz}} = 10\,\mathrm{Jy}$) and 3C454.3 ($S_{1.4\,\mathrm{GHz}} = 11\,\mathrm{Jy}$) as bandpass calibrators, as well as data from the same bandpass calibrators, 3C147 ($S_{1.4\,\mathrm{GHz}} = 23\,\mathrm{Jy}$) and 3C286 ($S_{1.4\,\mathrm{GHz}} = 15\,\mathrm{Jy}$) between several days. The noise level improvements were consistently near to theoretical expectations, and these examples represent a common trend in our results.

3.1   Example: Observing J0022+0014

To measure H I absorption in the direction of source J0022+0014 ($S_{1.4\,\mathrm{GHz}} = 3\,\mathrm{Jy}$) with RMS noise in H I optical depth of $\sigma_\tau = 5 \times 10^{-4}$ per $0.42\,\mathrm{km\,s^{-1}}$ channels, the VLA exposure calculator indicates that we need 12.5 hours of on-source integration time. Given that 21-SPONGE is a filler project, we needed to break this integration time requirement up into ≤ 1 hour scheduling blocks. We select source 3C48 ($S_{1.4\,\mathrm{GHz}} = 16.5\,\mathrm{Jy}$) as the bandpass calibrator for target J0022+0014, and J0022+0014 can perform as its own complex gain calibrator.

We received 11 executions of the same 1-hour scheduling block (SB) for J0022+0014: 5 between Februrary 13-18, 2014, and 6 between June 13-23, 2014. Each SB devoted 12 minutes to bandpass observations, which is a factor of 2 less than required to reach adequate sensitivity in the bandpass solution. Therefore, we combined all bandpass calibrator (i.e. 3C48) observations from each month of time ($\sim 7 - 10$ days each) to minimize the noise in the final BP solution, which we applied to all target observations from each month.

A comparison between the bandpass solution from a single observation (June 21, 2014) and the final, combined BP solution (all calibrator time from Jun 2014 combined) is shown in Figure 10. The

noise in amplitude and phase of the BP solution is visibly improved, demonstrating that remarkable stability is possible over long time intervals (10 days).

4   60 kHz Ripple

Given the high sensitivity of our calibration solutions, we identified a $\sim 60\,$kHz "ripple" present in all BP solutions, presented in VLA Memo #171 [3]. The ripple is caused by finite impulse response filters applied prior to correlation which shape the bandpass, and is stable in time (the period, amplitude and phase are constant between all examined solutions acquired all 4 years of observations) so that we are able to model and remove it after combining the observations.

Figure 11 displays the filter plus mixer response required to achieve the target H I sky frequency (courtesy K. Sowinski). The aforementioned ripple, caused by the 0.5 MHz filter, along with a small slope from the 8 MHz filter, is clearly evident.

To estimate the noise level in the BP solution independent of the ripple structure, we fit and remove the ripple outside of AIPS. Figure 12 displays an example of this modeling process. A zoom-in onto a bandpass solution from an observation of 3C147 is shown in the left panel, with the ripple model overlaid in red. The right panel displays the residuals following the removal the ripple model, from which the noise in the bandpass solution is computed.
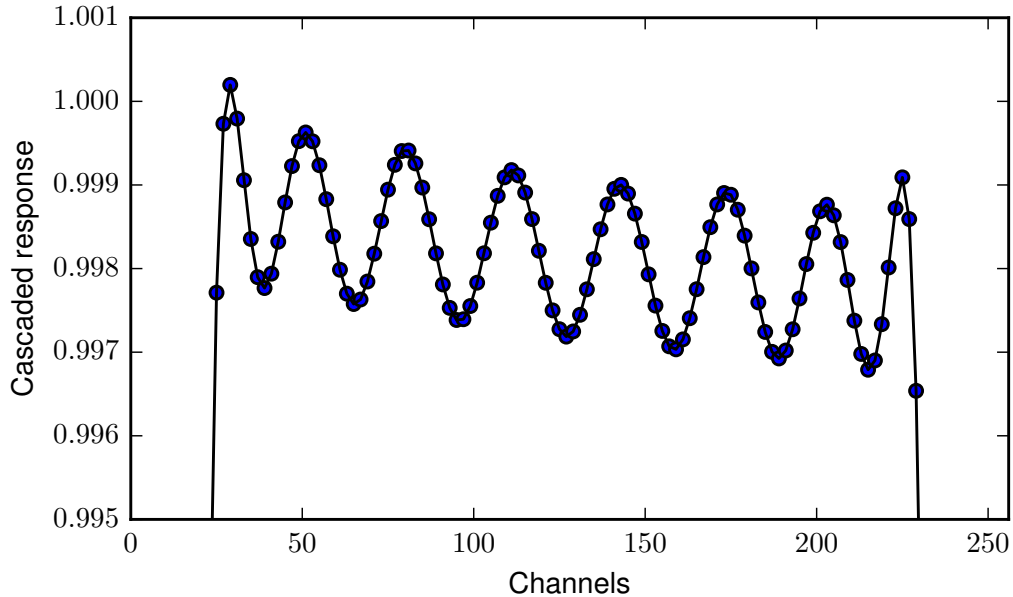

Figure 11: Cascaded response of all the filters and mixer needed to achieve the desired sky frequency and bandwidth for the subband containing the H I line (i.e. the "target" subband in Figure 1) vs. channels for a 21-SPONGE observation conducted on 2013/07/27. The 60 kHz ripple of the 0.5 MHz filter is evident, with a small slope from the 8 MHz filter (data courtesy K. Sowinski).
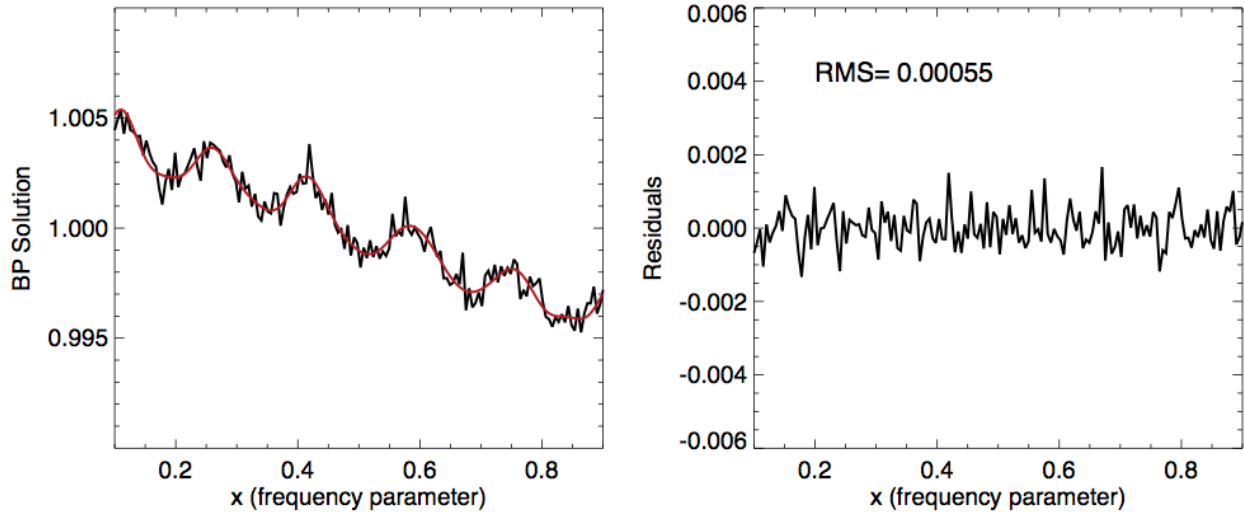
Figure 12: Zoomed-in BP solution (left) for an observation of soure 3C147 ($S_{1.4\,\mathrm{GHz}} = 23\,\mathrm{Jy}$) including the 60 kHz ripple, which we model (red) and subtract to produce residual BP solutions (right), from which we can estimate the RMS noise.

4.1 Effects of Improved Bandpass Stability

The upgrade to the expanded Very Large Array (EVLA) facilitated our ability to reach optical depth sensitivities below $\sigma_\tau = 10^{-3}$. This was demonstrated in Begum et al. (2010), and an example from their results is shown in Figure 13. The left panel of Figure 13 displays the absorption by HI in the direction of source 3C286 ($S_{1.4\,\mathrm{GHz}} = 15\,\mathrm{Jy}$) using only original VLA antennas, and the right panel
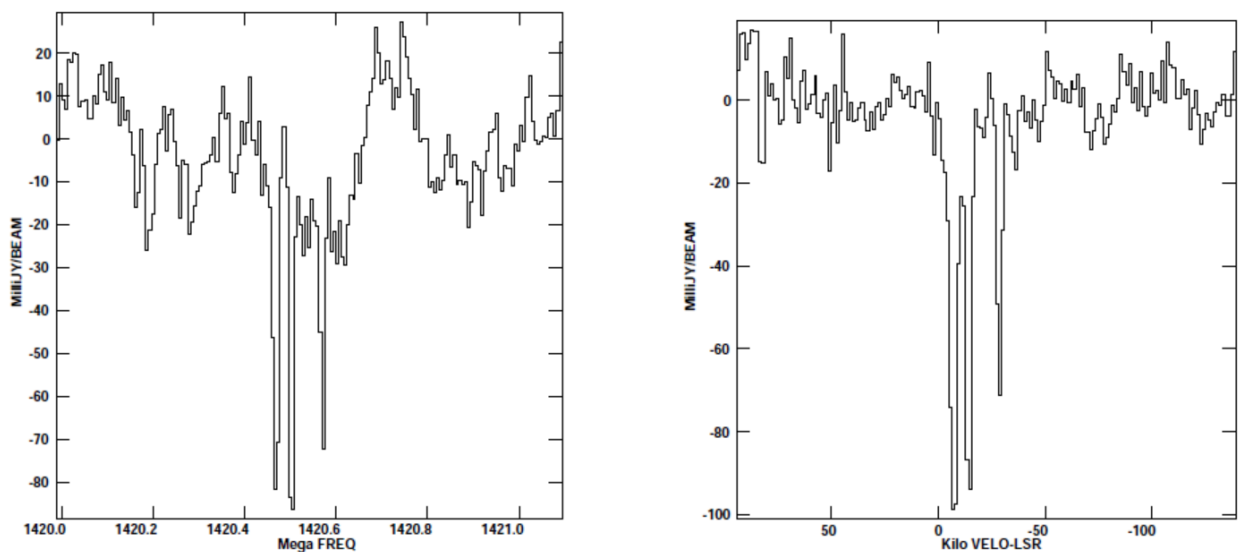

Figure 13: HI absorption spectra in the direction of 3C286 ($S_{1.4\,\mathrm{GHz}} = 15\,\mathrm{Jy}$). Left: Constructed using baselines from old VLA antennas (pre-upgrade). Right: Constructed using baselines from upgraded EVLA antennas.[1]
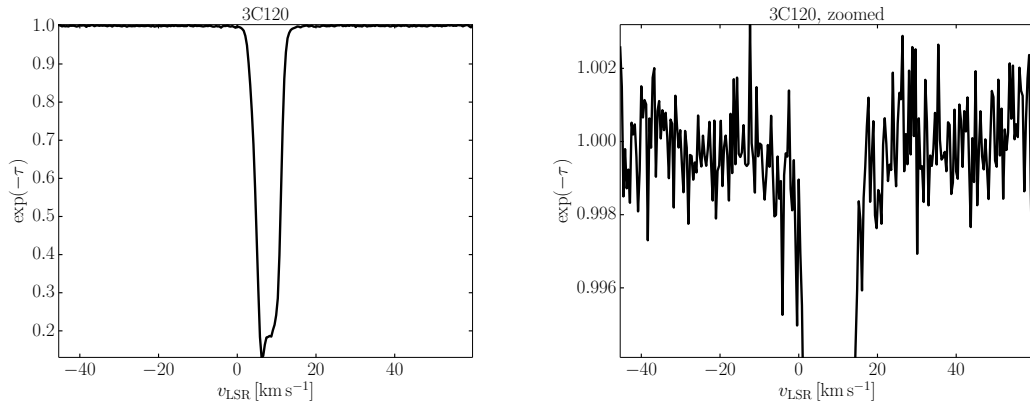
Figure 14: Left: 21-SPONGE Hɪ absorption spectrum in the direction of source 3C120 ($S_{1.4\,\mathrm{GHz}} = 4\,\mathrm{Jy}$). Right: zoom-in of same spectrum, to display the baseline structure. The RMS noise in optical depth per channel is 0.001.

displays the same spectrum using only upgraded EVLA antennas, and demonstrated remarkable improvement in baseline stability.

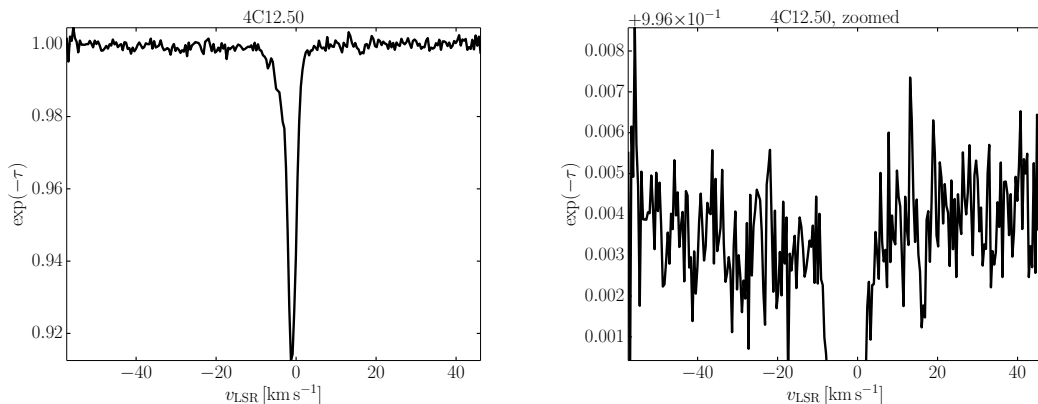### 4.1.1 Example 21-SPONGE Hi Absorption Spectra

Figure 15: Left: 21-SPONGE Hɪ absorption spectrum in the direction of source 4C12.50 ($S_{1.4\,\mathrm{GHz}} = 5\,\mathrm{Jy}$). Right: zoom-in of same spectrum, to display the baseline structure. The RMS noise in in optical depth per channel is 0.001.

Following the EVLA upgrade, and the availability of the WIDAR correlator, we were able to achieve similar stability in bandpass structure throughout the 21-SPONGE observations. Figures 14 through 16 display example 21-SPONGE Hɪ absorption spectra in the form: $\exp{-\tau(v)}$, where $\exp{-\tau(v)} = ((S_{1.4\,\mathrm{GHz}} + a(v))/S_{1.4\,\mathrm{GHz}})$, $a(v)$ is the continuum-subtracted absorption profile extracted from the central pixel of the AIPS-calibrated VLA data cube as a function of velocity, v ($0.42\,\mathrm{km\,s^{-1}}$ per channel resolution). The right panels zoom-in on the baseline structure. We consistently achieve RMS noise in $\tau(v)$ of $\sigma_\tau \sim 10^{-3}$ per channel. In all examples shown here, in addition to large-amplitude, narrow components, we find evidence for wide, low-amplitude, underlying Hɪ absorption features with FWHM $\sim 10\,\mathrm{km\,s^{-1}}$. These are detectable only because of the remarkable bandpass sensitivity and stability acheived by our observation and data reduction strategies.
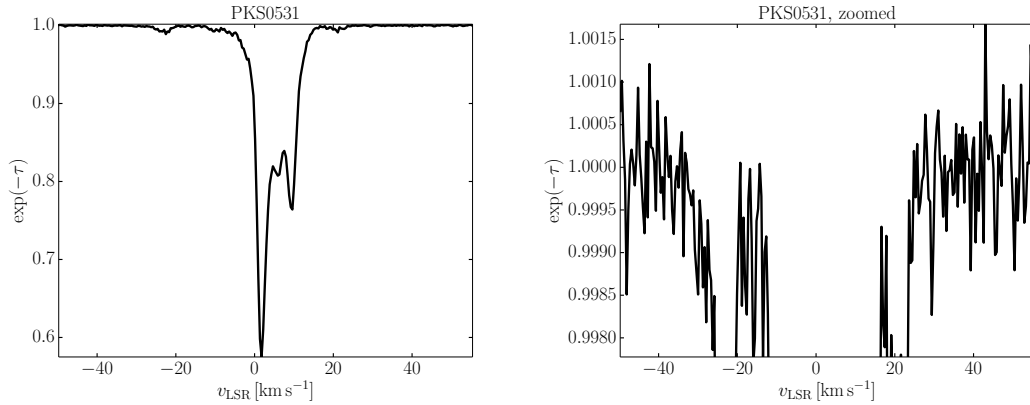
Figure 16: Left: 21-SPONGE H I absorption spectrum in the direction of source PKS0531+19 ($S_{1.4\,\mathrm{GHz}} = 7\,\mathrm{Jy}$). Right: zoom-in of same spectrum, to display the baseline structure. The RMS noise in in optical depth per channel is 0.0005.

5 Summary

For observations of Galactic H I with the VLA, we recommend the following calibration strategies:

- To avoid contamination by H I structure in the direction of calibrator sources, observe the calibrator source with two subbands, one at higher and one at lower frequencies, to compute bandpass solution via interpolation across the target frequencies. For our 0.5 MHz target subband setup, we used two subbands separated by 1.5 MHz respectively above and below the target H I line. We found that including additional subbands at increased separation from the target frequency did not improve the the calibration solution.

- To improve noise levels in calibrator solutions, we have found that it is possible to combine calibrator observations that are separateed in time by up to 10 days.

- To avoid resolving H I emission in the direction of background continuum sources observed for the purpose of detecting H I absorption, remove all baselines shorter than 300 m (or 1.4 kλ).

References

[1] Begum, A., et al., 2010, ApJ, 725, 1779B

[2] Kalberla, P. M. W., et al., 2005, A&A, 440, 775

[3] Murray, C. E., Goss, W. M., & Stanimirović, S., 2013, EVLA Memo 171. www.aoc.nrao.edu/evla/geninfo/memoseries/evlamemo171.pdf

[4] Murray, C. E., Goss, W. M., & Stanimirović, S., 2014, EVLA Memo 176. www.aoc.nrao.edu/evla/geninfo/memoseries/evlamemo176.pdf